

Tunable Thermal Transport and Mechanical Properties in Strained Graphene Nanoribbons

K.G.S.H. Gunawardana,^{*,†,⊥} Kieran Mullen,^{†,⊥} Jiuning Hu,^{‡,¶} Yong P. Chen,^{‡,§,¶}
and Xiulin Ruan^{‡,||}

Homer L. Dodge Department of Physics and Astronomy, The University of Oklahoma, Norman, Oklahoma 73069, USA, Birk Nanotechnology Center, Purdue University, West Lafayette, Indiana 47907, USA, School of Electrical and Computer Engineering, Purdue University, West Lafayette, Indiana 47907, USA, Department of Physics, Purdue University, West Lafayette, Indiana 47907, USA, and School of Mechanical Engineering, Purdue University, West Lafayette, Indiana 47907, USA

E-mail: harsha@ou.edu

Abstract

We study the effects of stress and strain on thermal transport and mechanical properties of armchair and zigzag graphene nanoribbons (AGNR and ZGNRs) using non-equilibrium molecular dynamics simulations. Both nanoribbons buckle at low temperatures (100K) and the buckling height decreases as the temperature increases. Moreover they experience an intrinsic tensile stress which decreases as the temperature increases. The thermal conductivity of AGNR

*To whom correspondence should be addressed

[†]Homer L. Dodge Department of Physics and Astronomy, The University of Oklahoma, Norman, Oklahoma 73069, USA

[‡]Birk Nanotechnology Center, Purdue University, West Lafayette, Indiana 47907, USA

[¶]School of Electrical and Computer Engineering, Purdue University, West Lafayette, Indiana 47907, USA

[§]Department of Physics, Purdue University, West Lafayette, Indiana 47907, USA

^{||}School of Mechanical Engineering, Purdue University, West Lafayette, Indiana 47907, USA

[⊥]Center for Semiconductor Physics in Nanostructures, The University of Oklahoma

decreases significantly with applied symmetric tensile strains below 0.1. On the other hand, thermal conductivity of ZGNR shows anomalous behavior we attribute to its small width. Asymmetric stress along the transport direction is achieved by exerting a lateral force F_y on the side atoms of one half of the AGNR. We observe significant thermal rectification up to 65% and interestingly, it is tunable with the F_y . The observed heat flux is larger from the less stressed region to the more stressed region than *vice versa*. This is a very promising approach for experimental realization of thermal rectification.

Operation of nano-scale thermal devices mainly relies on the tunability of phonon transport by external means. This has led to the emerging field called “phononics”.¹ These devices will be an essential part of future nano-electronics in thermal management, thermal logic applications and thermo-electric devices. The most fundamental thermal device is the thermal rectifier, in which the thermal transport is maximized in one direction. It has been shown theoretically that the structural asymmetry along with non-linearity of the force field are basic requirements for thermal rectification.²⁻⁴ Thermal rectification has been demonstrated in asymmetric one-dimensional (1D) systems by tuning the non-linearity using MD simulations.^{5,6} In a different approach, it has been shown that varying the mass across an atomic chain can produce a system that rectifies heat flux.⁷ The easy axis of thermal transport is in the direction of decreasing mass.

In experimentally realistic systems, Hu et al.⁸ and Yang et al.⁹ predict TR in triangular and trapezoidal shaped graphene nano-ribbons (GNRs). The favorable direction of thermal transport is always in the direction of decreasing the width. Moreover, the phenomena has been predicted in several interfaces of dissimilar non-linear materials.^{10,11} Chang et al. has made the first measurement of thermal rectification in asymmetrically mass loaded nanotubes.¹² They have observed increased thermal transport in the direction of decreasing mass and a thermal rectification factor (TR) up to 7%. In this work we introduce stress and strain as another aspect in realizing the thermal rectification in GNRs.

Graphene grown on a substrate is usually stressed and can be further strained or compressed using the thermal expansion of the substrate beneath it. The existence of negative thermal ex-

pansion coefficient (NTEC) of graphene is also an added advantage in this process.¹³ In addition, ripples may form in graphene due to mechanical instability¹⁴ or/and an artifact of the external stress.¹⁵ Further Bao et al.¹⁵ experimentally demonstrate the maneuverability of graphene ripples in orientation and size. The strained induced shifts of phonon frequencies of graphene 2D and G optical bands has been revealed recently using the Raman spectroscopy.¹⁶⁻¹⁸ Moreover, Raman spectroscopy is a vital tool in mapping the local strain on graphene. Therefore, with the development of these experimental tools, strain engineering in nano-scale is becoming a realizable goal.

In this work, we use non-equilibrium molecular dynamics (NEMD) method to study the effects of stress and strain on the thermal transport and thermal rectification in armchair and zigzag graphene nano-ribbons (AGNR and ZGNRs). First we give a short description of the simulation procedure, followed by the discussion of the studies on the temperature dependence of thermal conductivity, intrinsic stress and the mechanical behavior. Then we move to the core the work which describes the symmetric and asymmetric thermal transport under external stress. We observe asymmetric thermal transport after switching the bias when a non-uniform stress profile is exerted. This stress profile is achieved by applying a lateral force(F_y) on side atoms of one half of the AGNR. The choice of the application of F_y is such that the stress along the transport direction at the two edges, where the heat baths are applied, are different.(See [figure][4][4]) We observe a TR up to 65% and it is tunable with F_y as long as the stress is smaller than a limiting value that deforms the structure.

In the MD simulation, a second generation Brenner potential¹⁹ was employed to describe the interaction within the GNR. The MD code used in this calculation was first developed by Brenner²⁰ and further modified by Hu et al..⁸ We included some modifications to apply external forces, to strain and to calculate average forces on atoms. First, rectangular AGNR and ZGNR of dimensions $6.5 \text{ nm} \times 1.25 \text{ nm}$ and $6.4 \text{ nm} \times 1.15 \text{ nm}$ were constructed by setting the carbon-carbon bond length at 0.142 nm . The first and last columns of atoms were fixed and the adjacent four columns of atoms on both sides of AGNR and three columns of atoms on both sides of the ZGNR were coupled to Nosé -Hoover thermostats.^{21,22} (See the inset of [subfigure][1][1]1a) The equations of motions of

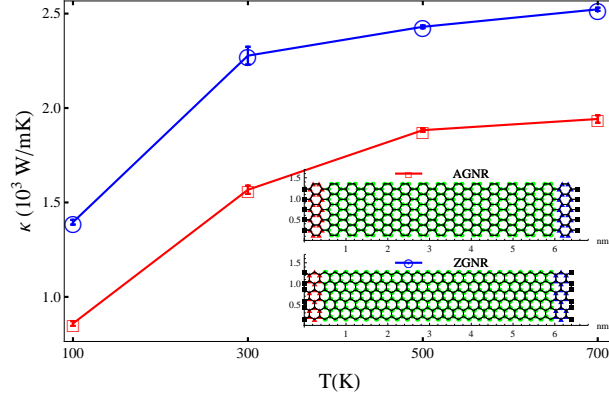
thermostated atoms are given by equation (1).

$$\begin{aligned} \frac{dP_i}{dt} &= F_i - \gamma P_i; & \frac{d\gamma}{dt} &= \frac{1}{\tau^2} \left(\frac{T(t)}{T_0} - 1 \right) \\ F_i &= -\sum_{k,l,j} \frac{\partial V_{kl}}{\partial r_{ij}} \end{aligned} \quad (1)$$

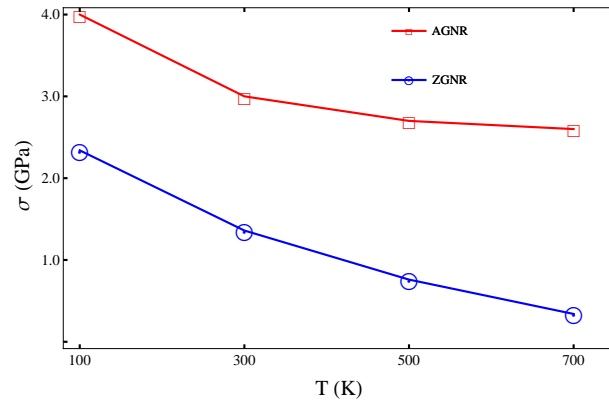
where, the subscript i runs over the atoms in either left or right thermostat, P_i is the momentum of the i -th atom, F_i is the force acting on the i -th atom, V_{kl} is the many-body potential, r_{ij} is the distance between atom i and j , γ and τ are the dynamic parameter and the relaxation time of the thermostat, $T(t) = \frac{2}{3Nk_B} \sum_i \frac{P_i^2}{2m}$, is the instantaneous temperature of the thermostat at time t , T_0 is the set temperature of the thermostat, N is the number of atoms in the thermostat, k_B is the Boltzmann constant and m is the mass of the carbon atom. Atoms not in the thermostats move according to standard Newtonian mechanics. These equation of motions are integrated by the third-order prediction-correction method. The time step is 0.5fs and the total simulation time is 5ns (10^7 time steps). The relaxation time of the thermostat (τ) is set to 1ps. The non-equilibrium steady state is reached after approximately 0.5ns and the measurements are taken from 2.5ns to 5.0ns.

The temperatures of the left and right heat baths (HBs) are set to T_L and T_R respectively, so that the average temperature (T) of the system is $T = (T_L + T_R)/2$ and the temperature difference is ($\Delta T = |T_L - T_R| = 2\alpha T$). The parameter $\alpha \approx 0.067$ is used in measuring thermal conductivity. The heat current injected from either the left(L) or right(R) Nosé-Hoover thermostat (J) is given by $J_{L/R} = \sum_i \frac{(-\gamma P_i) P_i}{m} = -3\gamma N k_B T(t)$. The net heat current at the steady state is $J = (J_L - J_R)/2$. The thermal conductivity (κ) of the system is calculated according to the Fourier's law $J = \kappa w h \frac{(T_L - T_R)}{d}$, where d , w and h are length, width and van der Waals thickness ($h = 0.335nm$) of the GNR.

First, the thermal conductivity (κ) of both AGNR and ZGNR is calculated in the temperature range 100K -700K ([subfigure][1][1]1a). The ZGNR shows higher thermal conductivity than the AGNR. At 300K thermal conductivity of AGNR is 1600 W/mK and that of the ZGNR is 2295 W/mK. The κ of both nanoribbons increases as the average temperature increases. Beyond 300K the rate of increase in the thermal conductivity with temperature is dramatically reduced. This could be a result of increased rate of phonon scattering from the boundaries and other phonons.



(a)



(b)

Figure 1: (a) Plot of thermal conductivity (κ) of ZGNR (Circle) and AGNR (Square) as a function of temperature. The insets are the schematics of the simulated AGNR and ZGNR. The full squares and triangles represent the atoms that are fixed and coupled to the Nosé-Hoover thermostats respectively. (b) Plot of tensile stress developed along the AGNR and ZGNR as temperature increased from 100 K to 700 K. This is calculated by taking the average force on the fixed atoms during the last 10^6 time steps.

During the simulation the time average of the forces on each atom, $\langle F_j \rangle_t$ for non-thermostatted atoms and $\langle F_i - \gamma P_i \rangle_t$ for thermostatted atoms, is calculated by averaging over the last 10^6 time steps. These time averaged forces are exponentially small except for the atoms at the two edges that are fixed. The externally applied force on the all fixed atoms on one side (holding them in fixed position) is always along the length direction of the GNR. There is an equal and opposite force on the fixed atoms acting on the center part of the nanoribbon. In fact this is the force developed across the nanoribbon. [subfigure][2][1]1b shows the stress(σ), force per unit area, developed along the GNR as a function of the temperature. The positive sign implies the stress is

tensile. The tensile stress can be attributed to the internal contraction of the GNR. Actually this is not an artifact of the imposed fixed boundary conditions. Relaxing the fixed atoms, by moving those inside, does not reduce the above stress. (See inset of [figure][2][2] for the effect at 300 K.) Both GNRs experience a tensile stress and it decreases as the temperature increases. Therefore the internal contractions are prominent at low temperature and reduce as temperature increases. In parallel to that AGNR shows buckling along the out of plane direction with a peak height of 0.15 nm at 100 K. As the temperature increases the peak height decreases and at 700 K it reaches 0.005 nm. But the ZGNR has a peak height about 0.03 nm and decreases only weakly with temperature. The experimentally observed peak height is higher than what we observe probably due to the small size of our simulated GNR. The buckling could be caused by the internal contraction forces due to the mechanical instability of this atomically flat membranes. We observe a reduction of the internal contraction forces as temperature increases and thus the GNR flattens.

By applying tensile/compressive strain ($\pm \frac{\Delta d}{d}$) flattening/bending of the GNR was observed. Strain was applied by slowly moving the fixed atoms on one side at a rate of $\pm 1.0 \times 10^{-7}$ nm per time step at the beginning of the simulation. At 300 K compressive strain of 0.03 show about 0.8 nm peak height for both AGNR and ZGNR. ([figure][2][2]) shows the variation of the stress with the applied strain on AGNR and ZGNR measured at 300 K. Both nanoribbons shows linear variation of stress with strain. By doing a linear fit we obtain the Young's modulus of AGNR to be 662 GPa and that of ZGNR to be 682 GPa. Similar values have been observed previously.^{23,24}

Thermal conductivity of AGNR significantly decreases under applied uniaxial tensile strain ([subfigure][1][3]3a). The reduction of thermal conductivity is about 45% at 0.1 strain. Ref.²⁶ and²⁷ have also observed a huge reduction in thermal conductivity under tensile strain. This is due to the lowering of the characteristic vibrational frequencies and the enhancement of the non-linearity with the tensile strain.²⁵ On the other hand compressive strain in the range of 0 to -0.03 results in a slight reduction of the thermal conductivity. This reduction is due to the buckling of the structure under the compressive strain, which is obvious because in this range of compressive strain there is no change of the stress along the nano ribbon (See the inset of [figure][2][2]).

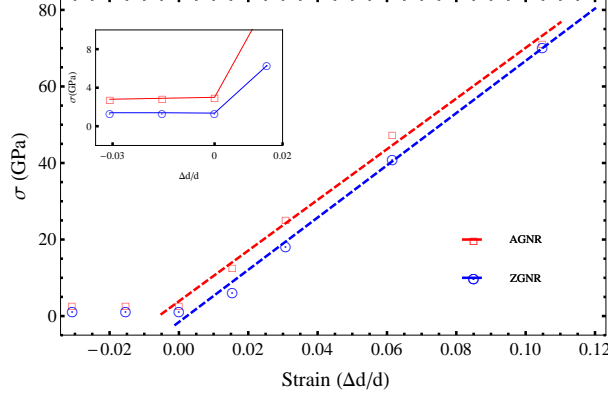
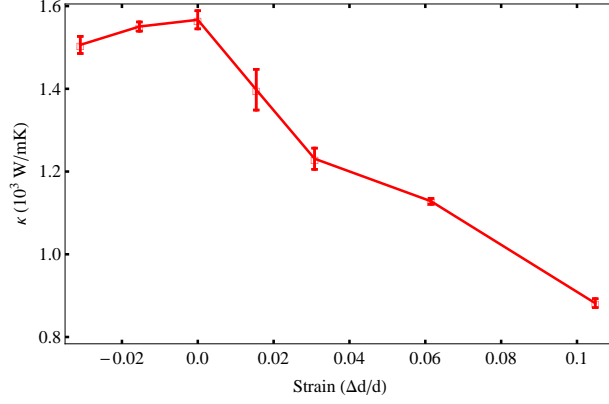


Figure 2: Plot of stress (in GPa) as a function of strain for AGNR(Square) and ZGNR (Circle) at room temperature (300 K). The dashed lines are the linear fit to the data of positive strain. From this we extract the Young’s modulus of AGNR to be 662 GPa and that of ZGNR to be 682 GPa. The Inset shows the variation of stress with the compressive strain in expanded scale. Note that there is no change of the stress in this range of compressive strain.

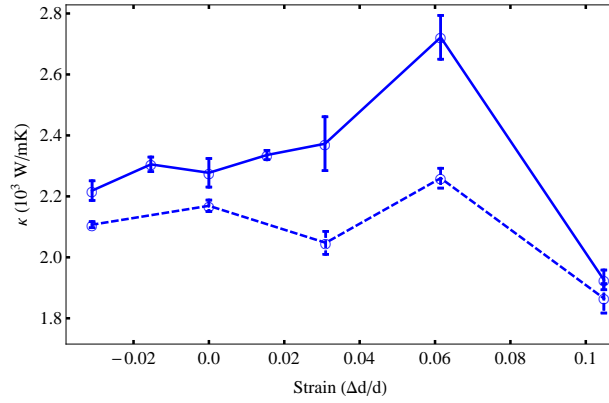
Therefore this procedure of applying compression is not a good approach to observe the effect of compressive stress, where we observe the enhancement of the thermal transport. Instead the Poisson contraction is recommended. On the other hand, thermal conductivity of ZGNR increases in the strain ranging from -0.03 to 0.06 . Further thermal conductivity shows a peak of 2722 W/mK at 0.06 strain ([subfigure][2][3]3b). We confirm this peculiar behavior is due to the small width ($w = 1.15$ nm) of the ZGNR. When the width is increased to 1.56 nm by adding two aromatic carbon rings, the peak height decreases to 2295 W/mK.(Dashed line in [subfigure][2][3]3b)

So far, we have considered the stress(σ) along the nanoribbon to be uniform. We now move to the case where it varies across the structure. Consider the stress at the left and right edges of the nanoribbon are σ_L and σ_R such that $\sigma_L \neq \sigma_R$. Now the heat baths have different phonon characteristics and also different coupling to the system. The above asymmetry, with the non-linearity in the force field satisfy the requirements for thermal rectification.² Below we describe the MD approach carried out to answer this question.

We now restrict our study to AGNR. The strain asymmetry is achieved by laterally stressing one half of the AGNR. As depicted in the [figure][4][4], a tensile force of magnitude F_y is applied on the upper and lower sides atoms of the right half of the AGNR . The tensile stress developed across the lateral direction (y) is denoted by σ_y . Hence a rough estimate of the required corresponding



(a)



(b)

Figure 3: Plot of thermal conductivity (κ) of AGNR (a) and ZGNR (b) as a function of Strain. This is calculated at 300 K with the bias of $\alpha = 0.3$. The strain was applied by slowly moving the fixed atoms on one side at a rate of $\pm 1.0 \times 10^{-7}$ nm per time step. The dashed line in (b) is for a wider ($w = 1.56$ nm) ZGNR.

strain can be made using the plot of stress vs. strain([figure][2][2]). This lateral stress produces a tensile strain along the y direction in the right half of the AGNR and, hence a compressive strain along the x direction due to the Poisson contraction. Since the atoms in the left and right edges are fixed this compressive force also results tensile stress in x direction near the HB. The magnitude of the stress near the left and right HBs are given by σ_L and σ_R and can be measured as previously. [table][1][1] shows the variation of σ_L and σ_R on F_y measured at 300 K. The magnitudes of σ_L and σ_R do not noticeably depend on α . The measured σ_L and σ_R are tensile, and σ_L is smaller than the σ_R while both are found to be increasing with F_y . However, when $F_y = 7.2$ nN, a large compressive stress of $\sigma_R = -74.0$ GPa is observed. This is due to the Poisson contraction along with the bond

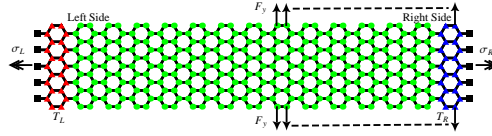


Figure 4: Schematic of the AGNR showing the applied forces. F_y is the force applied along the lateral direction on the side atoms (14 atoms on each side) of the right half of the AGNR. σ_L and σ_R are stress developed in x direction near the thermostats. T_L and T_R are the temperature of the left and right thermostats.

Table 1: Shows the variation of stress on the AGNR shown in the Fig. [figure][4][4]. F_y is the applied force on an atom in the lateral direction and the σ_y is the corresponding stress. σ_L and σ_R are the stress developed in x direction near the left and right thermostats. The σ_R is reasonable only near the right side HB. When moving to the center, it is more reduced due to the Poission contraction.

F_y (nN)	σ_y (Gpa)	σ_L (Gpa)	σ_R (Gpa)
2.4	38.8	4.8	10.7
4.0	64.8	7.2	16.7
4.8	77.7	8.3	19.1
5.6	90.7	9.6	22.7
7.2	116.6	15.5	-74.0

reconstruction occurred at the right side edge. (See the boxed region in [figure][5][5].) Since the contraction is comparably high, small ripples like structure on the right side edge was built up.

In [subfigure][1][6]6a, the forward bias (FB) and reverse bias (RB) thermal currents are plotted against the applied force F_y when $\alpha = 0.067$. As we expect with the tensile stress, both currents seem to decrease as we increase F_y . [subfigure][2][6]6b shows the thermal rectification factor(TR) against F_y . The TR was calculated using equation (2).

$$TR(\%) = 2 \frac{(J_{FB} - J_{RB})}{(J_{FB} + J_{RB})} \times 100\% \quad (2)$$

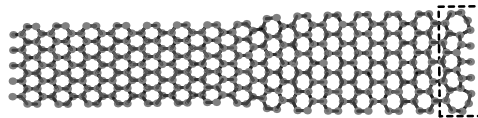


Figure 5: Top view of the AGNR shown in Fig. [figure][4][4] during the simulation when applied lateral force is $F_y = 7.2\text{nN}$. The boxed region shows the reconstruction of bonds which leads to large compressive force of $\sigma_R = -74.0$ GPa. The right side is wider than the left due to the strain.

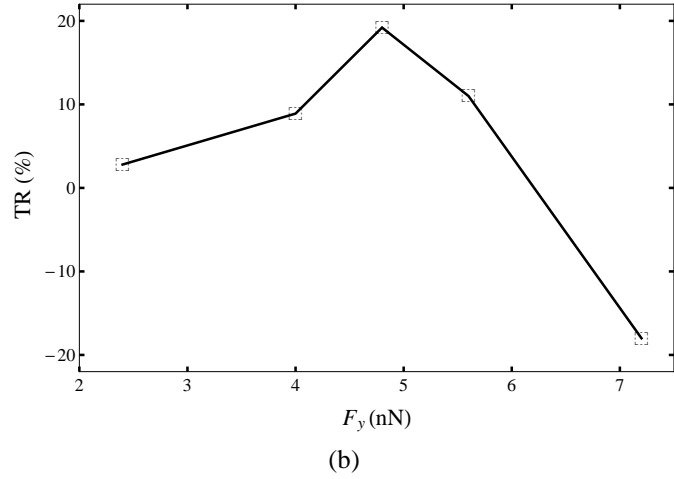
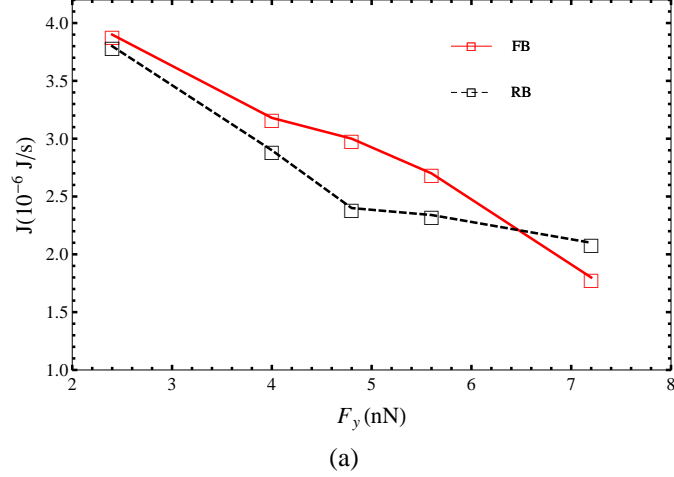
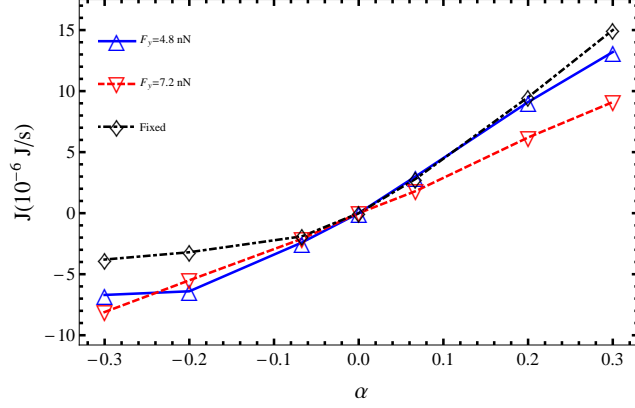
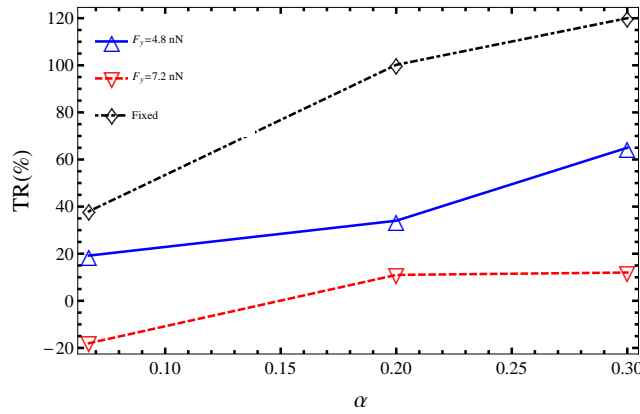


Figure 6: (a) Plot of FB(+ α ,Solid line) and RB(- α ,Dashed line) thermal currents as a function of applied lateral force F_y at $\alpha = 0.067$. The plot (b) is the corresponding TR vs. lateral force F_y at $\alpha = 0.067$.

The TR shows a peak of 20% when $F_y = 4.8$ nN and decreases down to -18% at $F_y = 7.2$ nN. This negative rectification could be due to the inverted profile of the stresses (σ_L and σ_R) near the thermostats ([table][1][1]). Further the TR can be improved as the bias (α) increases. [subfigure][1][7]7a shows the thermal currents against the bias α . When $F_y = 4.8$ nN (Solid line in [subfigure][1][7]7a) the FB thermal current linearly increases with the bias whereas, when the system is RB, the thermal current increases nonlinearly with the bias giving rise to larger TR of 65% at $\alpha = 0.3$. When $F_y = 7.2$ nN, the TR decreases down to 12% at $\alpha = 0.3$ (dashed line in [subfigure][1][7]7a). Therefore, when $F_y < F_L$, a limiting value that deform the structure, the observed thermal rectification is significant and can be tuned with the applied F_y .



(a)



(b)

Figure 7: (a) Plot of the FB ($+\alpha$) and RB ($-\alpha$) thermal currents as a function of bias (α) at the temperature $T_0 = 300$ K. The solid line is at $F_y = 4.8$ nN and dashed line is at $F_y = 7.2$ nN. The dotted (◇) line represent the case where the all side atoms are fixed with out applying any force. (b) Plot of thermal rectification factor (TR) as a function of bias (α)

It must be noted that the σ_R is reasonable only in the right HB region. When move towards the center it is more compressed due to the Poisson contraction. On the other hand σ_L is almost uniform in the left half except at the vicinity of the boundary between laterally stressed and free regions. We believe that this hindered the coupling of phonons from right HB to the interior region which eventually leads to the observed thermal rectification. When $F_y = 7.2$ nN the right side deforms in a way that compresses the atoms on to the fixed atoms. Now the coupling of phonons between right HB and the interior increases and the observed TR is reduced. Moreover the phonon population in either HBs could be different due to the asymmetry of the stress within the HBs. This would also make a significant contribution to the observed thermal rectification.

This kind of stress profile could be realized experimentally using the differential thermal expansion of the graphene on substrate, or by mounting the system on a piezoelectric material. Recently Chen et al.¹⁶ experimentally observed a compressive stress of the graphene on substrate region of partially suspended graphene over a trench on Si/SiO_2 substrate while the suspended region remain unaffected. Motivated by this, we believe that a thermal rectifier can be made by coupling the side atoms on which we apply lateral forces, on to a substrate that has a larger thermal expansion coefficient. In this case the lateral force is determined by the temperature of the substrate region. This would also create a difference in lateral force F_y over switching the bias which leads to further enhancement of the rectification. In addition to applying lateral forces this experimental set up would also have another effect, which is the reduction of the vibrational degree of freedom of the atoms coupled to the substrate. The dot-dashed (\diamond) line of [figure][7][7] is refer to the case that the side atoms on which the lateral force is applied are also fixed. This is analogous to strong coupling of the atoms to some heavy atoms. At this case there is no additional forces applied. Remarkably this results even larger thermal rectification, about 120% when $\alpha = 0.3$. It might be due to the reduction of the vibrational modes on the right hand side of the AGNR due to the fixed boundary condition along the lateral direction. Consequently the observable net thermal rectification could be even higher due to the coupling between the GNR and the substrate.

In conclusion, we study the effect of stress/strain on the thermal transport and thermal rectification of GNRs using NEMD simulations. We observe that both AGNR and ZGNR show buckling effects at low temperature (100K) and the buckling height decreases as the temperature increases. Moreover both GNRs experience a tensile stress, which is attributed to the internal contraction of the GNR, and decreases as the temperature increases. The thermal conductivity of AGNR decreases significantly with applied tensile strain which is less than 0.1. On the other hand, the thermal conductivity of ZGNR increases with strain and shows a peak around 0.06 strain. Interestingly the peak height has strong dependence on the width of the ZGNR. Asymmetric stress along the transport direction is achieved by exerting a lateral force F_y on the edge atoms of the right half on the AGNR. We observe thermal rectification up to 65%. The thermal current is larger from less

stress region to the more stress region than *vice versa*. We propose that a solid state thermal rectifier can be made by coupling the side atoms, on which we apply lateral forces, on to a substrate that has a larger thermal expansion coefficient.

Acknowledgement

This project was supported in part by the US National Science Foundation under Grant MRSEC DMR-0080054. JH and YPC acknowledge the support by NRI-MIND.

References

- (1) L. Wang, and B. Li, Physics World **21**, No.3, 27 (2008).
- (2) D. Segal, and A. Nitzan, Phy.Rev.Lett. **94**, 034301 (2005).
- (3) D. Segal, Phy.Rev.B **73**, 205415(2006).
- (4) L. A. Wu, and D. Segal, Phy.Rev.Lett. **102**, 095503(2009).
- (5) M. Terraneo, M. Peyrard, and G. Casati, Phys.Rev.Lett. **88**, No.9, 094302 (2002).
- (6) B. Li, L. wang, and G. Casati, Phys.Rev.Lett. **93**, No.18, 184301 (2004).
- (7) N. Yang, N. Li, L. Wang, and B. Li, Phy.Rev.B **76**, 020301 (R) (2007).
- (8) J. Hu, X. Ruan, and Y. P. Chen, Nano Lett. **9**, No.7, 2730-2735 (2009).
- (9) N. Yang, G. Zhang, and B. Li, Appl.Phys.Lett. **95**, 033107 (2009).
- (10) M. Hu, P. Keblinski, and B.Li, Appl.Phys.Lett. **92**, 211908 (2008).
- (11) M. Hu, J. V. Goicochea, B. Michel, and D. Poulikakos, Appl.Phys.Lett. **95**, 151903 (2009).
- (12) C. W. Chang, D. Okawa, A. Majumdar, and A.Zettl, Science **314**, 1121 (2006).
- (13) N. Mounet and N. Marzari, Phys. Rev. B **71**, 205214 (2005).

- (14) A. Fasolino, J.H. Los and M.I.Katsnelson, Nature materials **6**, 12 (2007).
- (15) W. Bao, F. Miao, Z. Chen, H. Zhang, W. Jang, C. Dames, C.N.Lau, Nature Nanotechnology **4**, 562-566 (2009).
- (16) C. C. Chen, W. Bao, J. Theiss, C. Dames, C. N. Lau, and S. B. Cronin, Nano Lett. **9**, No.12, 4172-4176 (2009).
- (17) M. Huang, H. Yan, C. Chen, D. Song, T. F. Heinz, and J. Hone, PNAS **106**, No.18, 7304-7308 (2009).
- (18) T. M. G. Mohiuddin, A. Lombardo, R. R. Nair, A. Bonetti, G. Savini, R. Jalil, N. Bonini, D.M.Basko, C.Galiotis, N. Marzari, K.S. Novoselov, A. K. Geim, and A.C. Ferrari, Phys.Rev.B **79**, 205433 (2009).
- (19) W.G.Brenner, phys.Rev. B **42**, 9458 (1990)
- (20) <http://www.eng.fsu.edu/~dommelen/research/nano/brenner/> .
- (21) S. J. Nosé, Chem.Phys. **81**, 511 (1984).
- (22) W. G. Hoover, Phys.Rev. A **31**, 1695 (1985).
- (23) C. D. Reddy, S. Rajendran, and K. M. Liew, Nanotechnology **17**, 864-870 (2006).
- (24) M. Arroyo, and T. Belytschko, Phy. Rev. B **69**, 115415 (2004).
- (25) R. C. Picu, T. B. Tasciuc, and M. C. Pavel, J. Appl. Phys. **93**, 3535 (2003).
- (26) Z. Guo, D. Zhang, and X. Gong, Appl. Phys. Lett. **95**, 163103 (2009).
- (27) X. Li, K. Maute, M. L. Dunn, and R. Yang, Phy. Rev. B **81**, 245318 (2010).